Model for thickness dependence of mobility and concentration in highly conductive zinc oxide

David C. Look
Kevin D. Leedy
Arnold Kiefer
Bruce Claflin
Naho Itagaki
Koichi Matsushima
Iping Suhariadi

Model for thickness dependence of mobility and concentration in highly conductive zinc oxide

David C. Look
Wright State University
Semiconductor Research Center
Dayton, Ohio
   and
Aerospace Division
Wyle Laboratories
Dayton, Ohio
   and
Sensors Directorate
Air Force Research Laboratory
Dayton, Ohio
E-mail: david.look@wright.edu

Kevin D. Leedy
Arnold Kiefer
Bruce Claflin
Sensors Directorate
Air Force Research Laboratory
Dayton, Ohio

Naho Itagaki
Koichi Matsushima
Iping Suhariadi
Kyushu University
Department of Information Science and Electrical
   Engineering
Fukuoka, Japan

Abstract. The dependences of the 294 and 10 K mobility μ and volume carrier concentration n on thickness ($d = 25$ to 147 nm) are examined in aluminum-doped zinc oxide (AZO). Two AZO layers are grown at each thickness, one with and one without a 20-nm-thick ZnON buffer layer. Plots of the 10 K sheet concentration n_s versus d for buffered (B) and unbuffered (UB) samples give straight lines of similar slope, $n = 8.36 \times 10^{20}$ and 8.32×10^{20} cm^{-3}, but different x-axis intercepts, $\delta d = -4$ and $+13$ nm, respectively. Plots of n_s versus d at 294 K produce substantially the same results. Plots of μ versus d can be well fitted with the equation $\mu(d) = \mu(\infty)/[1 + d^*/(d - \delta d)]$, where d^* is the thickness for which $\mu(\infty)$ is reduced by a factor 2. For the B and UB samples, $d^* = 7$ and 23 nm, respectively, showing the efficacy of the ZnON buffer. Finally, from n and $\mu(\infty)$ we can use degenerate electron scattering theory to calculate bulk donor and acceptor concentrations of 1.23×10^{21} cm^{-3} and 1.95×10^{20} cm^{-3}, respectively, and Drude theory to predict a plasmonic resonance at 1.34 μm. The latter is confirmed by reflectance measurements. © The Authors. Published by SPIE under a Creative Commons Attribution 3.0 Unported License. Distribution or reproduction of this work in whole or in part requires full attribution of the original publication, including its DOI. [DOI: 10.1117/1.OE.52.3.033801]

Subject terms: zinc oxide; mobility; thickness dependence; Hall effect; reflectance.

Paper 130129 received Jan. 25, 2013; revised manuscript received Feb. 25, 2013; accepted for publication Feb. 25, 2013; published online Mar. 13, 2013.

1 Introduction

Transparent conductive electrodes, typically formed from transparent conductive oxides (TCOs), are an important component of liquid crystal displays, solar cells, and light-emitting diodes.[1–4] The current leading TCO material is indium tin oxide (ITO), but its high cost has prompted a search for replacements, and a strong candidate is zinc oxide (ZnO) highly doped with Al, Ga, or In. ZnO has also recently been proposed as a plasmonic material in the near-infrared (IR) region, a range not accessible to noble-metal-based plasmonics.[5–10] The attractiveness of ZnO in these applications is partially due to the demonstrations of high-quality growth on many different substrates using many different growth techniques. However, a troubling problem is that films on lattice-mismatched substrates nearly always exhibit a thickness dependence of the electrical parameters, resistivity ρ, mobility μ, and carrier concentration n.[11–17] The origin of this problem seems to be connected with poor crystallinity near the substrate/layer interface. Recently, however, Itagaki et al.[16,18,19] have demonstrated significant improvement in the crystallinity of radio frequency (RF)-sputtered ZnO by inserting a thin ZnON buffer layer between the substrate and ZnO layer. For example, in undoped ZnO grown on c-plane aluminum oxide (Al$_2$O$_3$), the rocking-curve full width half maximum of the (002) diffraction drops from 0.490 to 0.061 deg, and

in Al-doped ZnO (AZO) grown on quartz-glass substrates, the thickness dependences of ρ, μ, and n greatly decrease. In the present work, we attempt to quantify these effects and understand their causes by carrying out detailed Hall effect and reflectance measurements and analysis. Among other things, we show that the measured thickness dependence of n is artificial and results from the electrical thickness d_{el} being different than the metallurgical thickness d (i. e., $d_{el} = d - \delta d$). As it turns out, the *true* value of n is independent of both thickness and the presence or absence of the buffer, as confirmed by reflectance measurements in the plasmonic region. On the other hand, the measured thickness dependence of mobility (and thus resistivity) is not artificial and results from the presence of interface scattering, which has a stronger effect on electrons in thinner samples. Finally, as a general result of this study, we introduce a new figure of merit d^* to describe interface quality. This quantity is defined by $\mu(d^* - \delta d) = \mu(\infty)/2$, where d^* and $\mu(\infty)$ are fitting parameters in the formula $\mu(d) = \mu(\infty)/[1 + d^*/(d - \delta d)]$. Essentially, for $d < d^* + \delta d$, interface scattering dominates all other scattering mechanisms; thus, a good interface has a low value of d^*. We find that $d^* = 23$ nm for the unbuffered (UB) samples, and only 7 nm for the buffered (B) samples. Also, from the values of n and $\mu(\infty)$, we can use degenerate electron scattering theory to determine donor and acceptor concentrations.

2 Experiment

AZO layers of thickness 25 to 147 nm were deposited by RF magnetron sputtering on quartz-glass substrates. For each thickness, one AZO layer was grown on a bare substrate, and another on a substrate with a 20-nm-thick ZnON buffer layer, deposited by RF magnetron sputtering at 300°C in $4/20.5$ [sccm] N_2/Ar ambient, producing a total pressure of 0.35 Pa. The targets for the buffers were 99.99%-pure ZnO, and the applied RF power was 100 W. The AZO films themselves were grown at 200°C in pure Ar ambient using ZnO targets with 2 wt%Al_2O_3. Although the buffer layers in this case were 20-nm thick, results have been shown to be substantially the same with thicknesses from 5 to 100 nm. Electrically, they are semi-insulating and have minimal direct effect on the conductivity of the AZO layer on top. The purpose of the N in the buffer layer is to inhibit the strong nucleation tendency of ZnO, which leads to small grain sizes. Indeed, x-ray diffraction $\omega - 2\theta$ scans indicate an increase in grain size from 38 to 68 nm due to the buffer. Further details on growth and structural analysis can be found in Refs. 16, 18, and 19.

Hall-effect measurements were carried out in a LakeShore 7507 apparatus. The magnetic field strength was 1 T and the temperature range, 6 to 320 K. The samples were of size 1×1 cm, and ohmic indium dots were placed at the four corners. Spectroscopic reflectance measurements were performed in a Perkin-Elmer Lambda 900 UV/Vis spectrometer at 294 K and over a wavelength range 190 to 3200 nm (6.52 to 0.39 eV).

3 Mobility Model

We have previously developed a general mobility model for degenerate electrons in semiconductor materials.[20] For purposes of the present paper, that model can be summarized as:

$$\mu(n, T, d_{el})^{-1} = \mu_{bulk}(n, T)^{-1} + \mu_{bdry}(n, d_{el})^{-1}, \quad (1)$$

where μ_{bulk} includes contributions from all bulk scattering mechanisms, such as lattice vibrations and ionized impurities, and

$$\mu_{bdry}(d_{el}, n, C) = \frac{e}{m^*} \frac{d_{el}/C}{\nu_{Fermi}(n)} = \frac{e}{\hbar} \frac{d_{el}/C}{(3\pi^2 n)^{1/3}}, \quad (2)$$

where C is a constant of order unity. Here d_{el} is the electrical thickness, i.e., $d_{el} = d - \delta d$, where d is the metallurgical thickness and δd is the thickness of a depletion layer, if any. As an example, $C = 2.5$ and $\delta d \sim 17$ nm in some Ga-doped ZnO samples grown by pulsed laser deposition in another laboratory.[14,20] One hypothesis in this simple mobility model is that the donor N_D and acceptor N_A concentrations (and thus $n = N_D - N_A$) do not vary with depth. Indeed, it should be pointed out that there are many instances in which this hypothesis may be violated. For example, in an ion-implanted sample, the concentration of ions, and thus the resulting μ and n, will usually vary with depth. However, for our samples we will explicitly show that n is not a function of depth so that all of the depth dependence of μ is contained in the d_{el} term in Eq. (2). Then Eq. (1) can be written as:
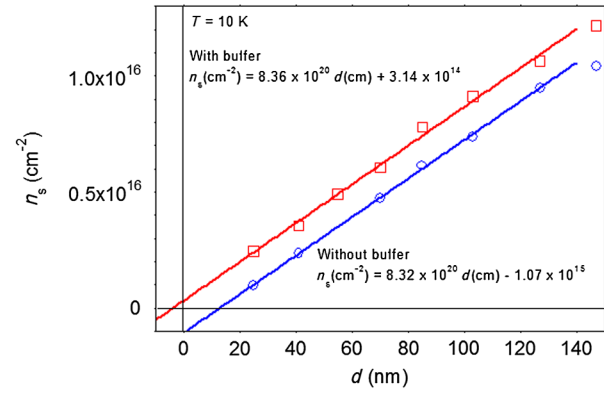

Fig. 1 The sheet carrier concentration n_s at 10 K versus thickness d for unbuffered and buffered samples. In each case, the slope is the volume carrier concentration n and the y-axis intercept is the excess electronic charge. The buffered sample has an *additional* electronic charge of 3.14×10^{14} cm^{-2}, while the unbuffered sample has a *deficit* of 1.07×10^{15} cm^{-2}.

$$\mu(d, \delta d)^{-1} = \mu_{bulk}^{-1} + \mu_{bdry}(d, \delta d)^{-1} = \mu_{bulk}^{-1} \left[1 + \frac{\mu_{bulk}}{\mu_{bdry}(d, \delta d)} \right]$$

$$= \mu_{bulk}^{-1} \left[1 + \frac{d^*}{d - \delta d} \right]. \quad (3)$$

Noting that $\mu_{bulk} = \mu(\infty)$, we can finally write Eq. (3) as

$$\mu(d) = \frac{\mu(\infty)}{\left[1 + \frac{d^*}{d - \delta d} \right]}. \quad (4)$$

Here the formal definition of d^* as a function of n, $\mu(\infty)$, and C can be found from Eqs. (2) and (3), but for our purposes it simply replaces C as a fitting parameter in a $\mu(d)$ versus d plot. The only other fitting parameter is $\mu(\infty)$, since δd is found from the intercept of a sheet concentration n_s versus d plot (Fig. 1). The motivation in fitting $\mu(d)$ to Eq. (4), rather than Eq. (1), is that d^* has practical significance as the thickness at which the maximum possible mobility, $\mu(\infty)$, has dropped by half; i.e., $\mu(d^* - \delta d) = \mu(\infty)/2$. In this regard, the value of d^* can be used as a figure of merit for the effects of interfaces on mobility.

4 Experimental Results and Analysis

In our study, the measured values of ρ, μ, and n vary as a function of metallurgical thickness d, consistent with the results of many other studies.[11–17] However, it must be remembered that ρ and n (but not μ) require knowledge of the electrical thickness d_{el}, which may not be the same as d. That is, the Hall effect does not directly measure a volume concentration n (cm^{-3}), but a sheet concentration n_s (cm^{-2}). If n is uniform, then these two quantities are simply related by $n = n_s/d_{el}$, where $d_{el} = d - \delta d$ is the electrical thickness, the region that contains free electrons. (If n is not uniform, then n_s is an averaged quantity,[21] not of importance here.) If $\delta d \ll d$, then $d_{el} \approx d$, as is usually assumed; however, in very thin samples there may be depleted regions that cover a significant fraction of the total thickness, so that $d_{el} \neq d$. To test this possibility, we plot n_s versus d, shown in

Fig. 1. Both B and UB samples display straight lines of slope $n = 8.36 \times 10^{20}$ cm^{-3}, showing immediately that the bulk n is *not* a function of depth or of the quality of the interface, at least for $d > 25$ nm. (In our calculations, we will ignore the slight difference in the slopes of the two lines.) But the intercepts of the B and UB lines differ significantly. The UB samples have a y-axis intercept of $\delta n_s = -1.07 \times 10^{15}$ cm^{-2}, and an x-axis intercept of $\delta d = +13$ nm. Thus, the electrical thickness is $d_{el} = d - 13$ nm, so that $n(d) = n_s(d)/(d - 13)$, not $n_s(d)/d$. Similarly, the resistivity is now given by $\rho(d) = \rho_s(d) \cdot (d - 13)$, not $\rho_s(d) \cdot d$. These *renormalized* ρ, μ, and n points for the UB samples are plotted in Fig. 2, and it is seen that indeed, most of the n points fall very close to the straight dashed line $n = 8.36 \times 10^{20}$ cm^{-3}; thus, when properly normalized, n is independent of thickness. Note also that $n(10$ K$) \approx n(294$ K$)$, showing that the electrons are truly degenerate.

We now examine n_s versus d for the B samples, also plotted in Fig. 1, and see that this line has the same slope as that of the UB samples, but not the same intercepts. Indeed, the B samples have $\delta n_s = +3.14 \times 10^{14}$ cm^{-2}, and $\delta d = -4$ nm. Thus $d_{el} = d - \delta d = d + 4$. This result can perhaps be understood as a slight diffusion of Al into the ZnON buffer that thereby increases the effective electrical thickness of the AZO layer. However, we should be cautious about any final explanations in this case because δd is small enough that a slight change in slope would make a large percentage change in δd. The renormalized ρ, μ, and n versus d results for the B samples are plotted in Fig. 3, and it is again seen that $n = n_s/(d + 4)$ is constant with thickness and moreover has the same magnitude as that of the UB samples. We also see that μ has a much smaller thickness dependence, showing that the buffer is very effective in this regard.

From the data and analysis so far, we can draw three conclusions: (1) the volume concentration n does not depend on metallurgical thickness d for either B or UB samples; (2) moreover, n does not depend on the presence or absence of the buffer; and (3) the mobility μ *does* depend on d, and it *does* depend on the buffer. If we had no other knowledge, the simplest explanation for (3) would be that N_D and N_A are varying with d because it is well known that μ is a strong function of these quantities in heavily doped
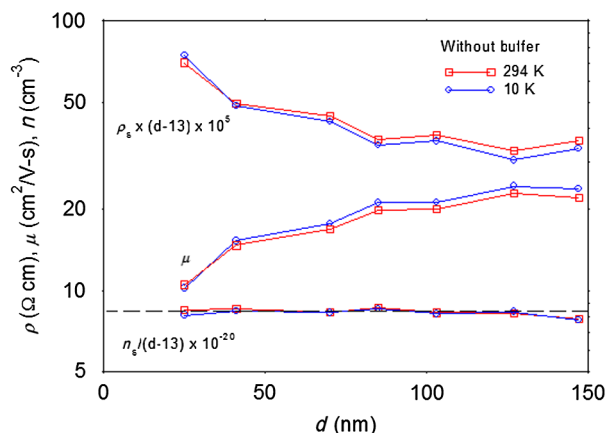

Fig. 3 The resistivity ρ, mobility μ, and carrier concentration n as a function of metallurgical thickness d for the buffered sample. Here n and ρ are normalized to the electrical thickness $d_{el} = d + 4$ nm; i.e., $n = n_s/(d + 4)$, and $\rho = \rho_s \times (d + 4)$.

materials. But this possibility is unlikely because N_D and N_A would then have to track each other exactly in order to maintain a constant $n = N_D$-N_A. A more likely explanation is that interface scattering is occurring and that electrons in thinner samples will scatter more from the interface because they are closer to it on the average. This latter explanation is strongly supported by the fact that Eq. (4) gives a good fit to the data.

The μ versus d data for the B and UB samples at 10 and 294 K are plotted in Figs. 4 and 5, respectively, and fitted to Eq. (4), $\mu(d) = \mu(\infty)/[1 + d^*/(d - \delta d)]$, where $\delta d = -4$ and $+13$ nm for the B and UB samples, respectively. For both B and UB samples, $\mu(\infty) = 27.6 \pm 0.3$ cm^2/V-s at 10 K, and 25.5 ± 0.2 cm^2/V-s at 294 K; and for both 10 and 294 K, $d^* = 6.9 \pm 0.2$ nm for the B samples, and 23 ± 1 nm for the UB samples. By applying the mobility theory in Ref. 20 to n and $\mu(\infty)$, we get $N_D = 1.23 \times 10^{21}$ cm^{-3} and $N_A = 1.97 \times 10^{20}$ cm^{-3} from the data at 10 K, and $N_D = 1.23 \times 10^{21}$ cm^{-3} and $N_A = 1.95 \times 10^{20}$ cm^{-3} from the data at 294 K, values very consistent with each other. In these calculations, we have assumed that the dominant acceptor has a

Fig. 2 The resistivity ρ, mobility μ, and carrier concentration n as a function of metallurgical thickness d for the unbuffered sample. Here n and ρ are normalized to the electrical thickness $d_{el} = d - 13$ nm; i.e., $n = n_s/(d - 13)$, and $\rho = \rho_s \times (d - 13)$.

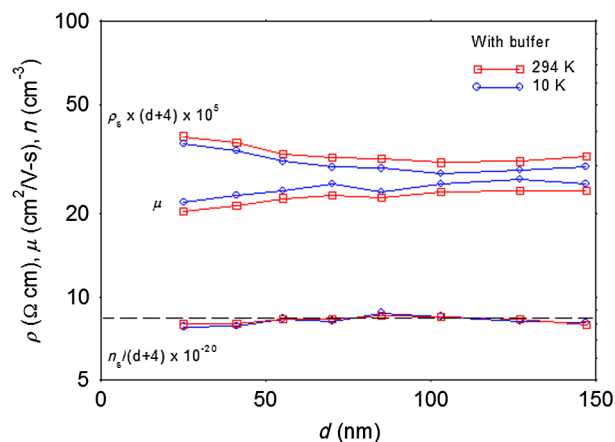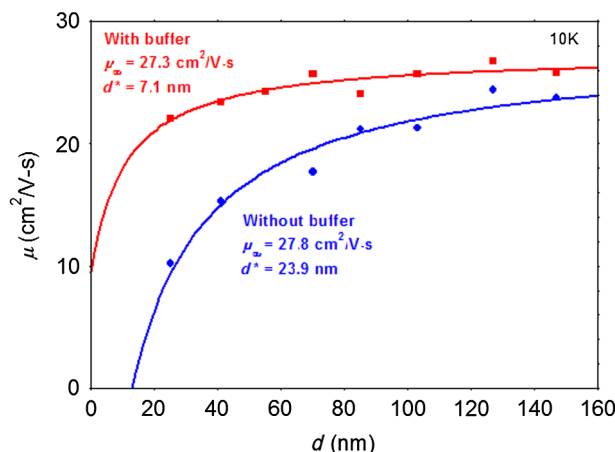**Fig. 4** The mobility μ as a function of metallurgical thickness d at 10 K. The parameters $\mu(\infty)$ and d^* result from a fit of Eq. (4): $\mu(d) = \mu(\infty)/[1 + d^*/(d - \delta d)]$, where $\delta d = -4$ and $+13$ nm for the buffered and unbuffered layers, respectively.
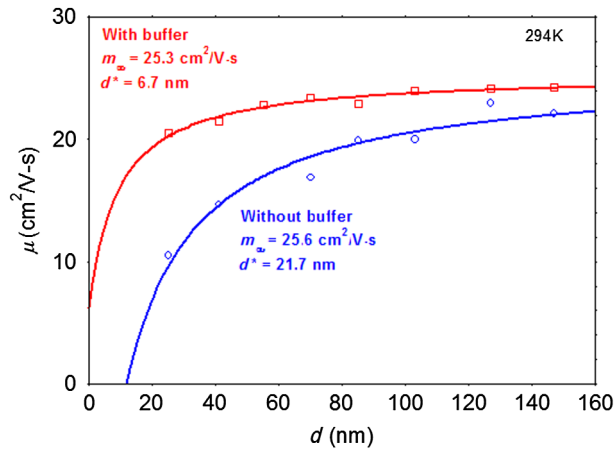
Fig. 5 The mobility μ as a function of metallurgical thickness d at 294 K. The parameters $\mu(\infty)$ and d^* result from a fit of Eq. (4): $\mu(d) = \mu(\infty)/[1 + d^*/(d - \delta d)]$, where $\delta d = -4$ and $+13$ nm for the buffered and unbuffered layers, respectively.
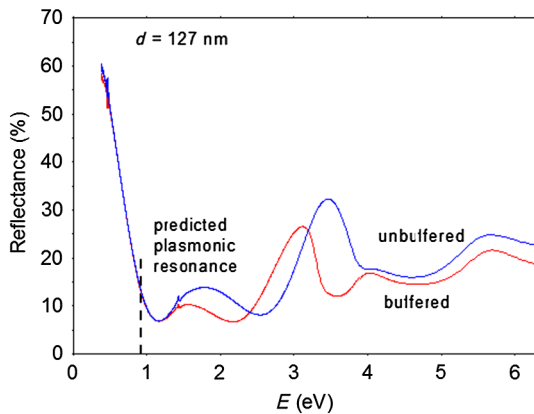

Fig. 6 Reflectance versus energy for the buffered and unbuffered samples of thickness 127 nm. The plasmonic resonance energy predicted from the Hall-effect results is shown as a vertical dashed line.

charge of 2, because it is likely the Zn vacancy.[20] The donors, of course, are assumed to consist mainly of Al_{Zn} impurities (charge 1), although no analytical measurements have been performed as yet.

The efficacy of the ZnON buffer layer is clear from a comparison of μ versus d in Figs. 2 and 3. In more quantitative terms, we have values $d^* = 7$ nm for the B samples and 23 nm for the UB samples. From the definition $\mu(d^* - \delta d) = \mu(\infty)/2$, this means that a 294 K mobility of $25.5/2 = 12.8$ cm^2/V-s could be reasonably expected in a buffered sample of metallurgical thickness $d = 7 - 4 = 3$ nm and in an UB sample of $d = 23 + 13 = 36$ nm. Even though the B value of 3 nm is not very accurate because of the inaccuracy in δd, still it is clear that the buffer makes it possible to grow very thin AZO layers that are conductive.

An example of reflectance data, for the B and UB samples of thickness 127 nm, is given in Fig. 6. From the values of n and $\mu(\infty)$, a plasmonic resonance energy of 0.925 eV (1.34 μm) can be predicted[10] and is indicated in the figure. Indeed, this energy is close to the threshold of the strong reflectance due to the plasmons. Interestingly, the resonance wavelength of 1.34 μm is near one of the major low-

absorption regions in optical fibers used in telecommunications. Note also in Fig. 6 that the reflectances of the buffered and UB samples are nearly identical in the plasmonic region, further affirming that the presence or absence of the buffer does not affect n.

5 Summary

We have analyzed the effects of a ZnON buffer layer on the electrical properties of thin Al-doped ZnO films grown by RF sputtering on quartz glass substrates. The volume carrier concentration n is independent of thickness d over the range 25 to 147 nm and is also not affected by the presence of the buffer. However, the mobility μ is strongly influenced by the buffer, exhibiting decreased thickness dependence and increased magnitude at a given thickness. Theoretical analysis shows that the observed lower mobility in thinner AZO layers, especially in those without a buffer, is due to increased scattering at the interface because the electrons are closer to it. The effect of the ZnON buffer is to reduce this scattering and also to reduce or eliminate the trapping at the interface of free electrons from the bulk. From the values of n and $\mu(\infty)$, donor and acceptor concentrations are calculated as 1.23×10^{21} and 1.97×10^{20} cm^{-3}, respectively. From these same values, a plasmonic resonance wavelength of 1.34 μm is predicted and is confirmed by reflectance measurements.

References

1. T. Minami, "Transparent conducting oxide semiconductors for transparent electrodes," *Semicond. Sci. Technol.* **20**(4), S35–S44 (2005).
2. D. C. Look, "Recent advances in ZnO materials and devices," *Mater. Sci. Eng. B* **80**(1–3), 383–387 (2001).
3. S. J. Pearton et al., "Recent progress in processing and properties of ZnO," *Prog. In Mater. Sci.* **50**(3), 293–412 (2005).
4. U. Ozgur et al., "A comprehensive review of ZnO materials and devices," *J. Appl. Phys.* **98**(4), 041301 (2005).
5. M. A. Noginov et al., "Plasmonic materials for telecom wavelengths," *Appl. Phys. Lett.* **99**(2), 021101 (2011).
6. J. A. Dionne and H. A. Atwater, "Plasmonics: metal-worthy methods and materials in nanophotonics," *MRS Bull.* **37**(8), 717–724 (2012).
7. P. R. West et al., "Searching for better plasmonic materials," *Laser Photon. Rev.* **4**(6), 795–808 (2010).
8. J. B. Khurgin and A. Boltasseva, "Reflecting upon the losses in plasmonics and metamaterials," *MRS Bull.* **37**(8), 768–779 (2012).
9. D. C. Look, T. C. Droubay, and S. A. Chambers, "Stable highly conductive ZnO via reduction of Zn vacancies," *Appl. Phys. Lett.* **101**(1), 102101 (2012).
10. D. C. Look, T. C. Droubay, and S. A. Chambers, "Optical/electrical correlations in ZnO: the plasmonic resonance phase diagram," *Phys. Status Solidi* (submitted).
11. T. Minami, "Transparent conducting oxide semiconductors for transparent electrodes," *Semicond. Sci. Technol.* **20**(4), S35–S44 (2005).
12. A. Suzuki et al., "Ultrathin Al-doped transparent conducting zinc oxide films fabricated by pulsed laser deposition," *Thin Solid Films* **517**(4), 1478–1481 (2008).
13. T. Minami and T. Miyata, "Present status and future prospects for development of non- or reduced-indium transparent conducting oxide thin films," *Thin Solid Films* **517**(4), 1474–1477 (2008).
14. D. C. Look et al., "Mobility analysis of highly conducting thin films: application to ZnO," *Appl. Phys. Lett.* **96**(6), 062102 (2010).
15. T. Yamada et al., "Ingrain and grain boundary scattering effects on electron mobility of transparent conducting polycrystalline Ga-doped ZnO films," *J. Appl. Phys.* **107**(12), 123534 (2010).

16. N. Itagaki et al., "Highly conducting and very thin ZnO:Al films with ZnO buffer layer fabricated by solid phase crystallization from amorphous phase," *Appl. Phys. Exp.* **4**, 011101 (2011).
17. B. L. Zhu et al., "Thickness study of AZO films by RF sputtering in Ar + H$_2$ atmosphere at room temperature," *Phys. Stat. Solidi A* **209**(7), 1251–1258 (2012).
18. N. Itagaki et al., "Novel fabrication method for ZnO films via nitrogen-mediated crystallization," *Proc. SPIE* **8263**, 826306 (2012).
19. K. Kuwahara et al., "High quality epitaxial ZnO films grown on solid-phase crystallized buffer layers," *Thin Solid Films* **520**(14), 4674–4677 (2012).
20. D. C. Look et al., "Self-compensation in semiconductors: the Zn vacancy in Ga-doped ZnO," *Phys. Rev. B* **84**(4), 115202 (2011).
21. D. C. Look, "Two-layer Hall-effect model with arbitrary surface-donor profiles: application to ZnO," *J. Appl. Phys.* **104**(6), 063718 (2008).

Biographies and photographs of the authors are not available.